Image and Observer Regions in 3D Displays

Vladimir Saveljev*

Abstract

The relation between light sources and screen cells is considered part of the theoretical model of an autostereoscopic 3D display. The geometry of the image and observer regions is presented, including the cases of single and multiple regions. The characteristic function is introduced. Formulas for the geometric parameters are obtained, including areas and angles. Special attention is drawn to the screen location. The method of transforming the formulas between regions is stated. For multiple regions, geometric dissimilarity was found. This allows the model to be applied in finding the geometric characteristics of multiview and integral-imaging 3D displays.

Keywords: 3D display, autostereoscopic, integral imaging, multiview imaging, geometric model

1. Introduction

Many research works on 3D displays are being published today. A detailed comparison can be found in [1-5] and in the references therein. Papers [6-8] represent the state-of-the-art 3D display technology. Most of the papers that were used as references herein focus on particular devices and their special features. These issues are very important in developing new 3D display devices and in demonstrating their abilities. On the other hand, in some of the papers used as references herein, the authors built or used models of 3D displays or their essential parts [9-14]. For the present paper, these model-related papers are of utmost interest because some common properties of displays are described therein.

In particular, model [9] describes a recording system based on a hexagonal lens array. Many important formulas were found by these authors, including disparity and the spread function. [10] is a homogeneous-matrix-based model describing the perceived depth range, including the fusion limitations. Stern and Javidi [11] clearly classified integral-imaging displays and analyzed an ideal display. [12] and [13] analyzed the following particular issues of integral-imaging and multiview displays: viewing angle, depth, and angular resolution. [14] is based on the lenslet model. At the same time, none of the listed papers builds an extendable model that may cover a variety of displays and may involve various non-ideal circumstances while keeping the main core of the model.

These authors' model of an autostereoscopic 3D display was built to satisfy the above conditions. In the model, no distinction was made between the integral-imaging and multiview displays, and both classes were assumed to satisfy more general conditions [15]. The model is basically presented in [16]. It involves a display device consisting of two layers: the image screen and an array of light sources or their optical equivalents (lenses or pinholes). In this paper, the term "point light source" is constantly used even if "pinholes" (arranged in a pinhole array) or "lenses" (lenslet array) can instead be used. The description of the model [16] is given in the projective form, but in this paper, the regular Euclidean form was mostly used.

In the current study, the regular tessellations (tilings) and the corresponding light source arrays were analyzed, the geometric relationships for single (central, main) regions were obtained, two particular cases related to the screen location were involved, and multiple regions were considered. The method of transforming formulas is described in this paper.

2. Screen Cells

Generally, a screen is a transparent or light-emitting

Manuscript Received March 13, 2010; Revised June 17, 2010; Accepted for publication June 22, 2010
* Member, KIDS
Corresponding author: Vladimir Saveljev
Research Institute of Electrical and Computer Engineering, Hanyang University
Room 408 HIT, Hanyang University, 17 Haengdang-dong, Seongdong-gu, Seoul 133-791, Republic of Korea
E-mail: saveljev@hanyang.ac.kr **Tel:** +82-2-2294-0618 **Fax:** +82-2-2294-0619

physical device that is used to create a uniform structure. In a 3D display, the image screen is logically divided into cells with no physical boundaries between them. Nevertheless, the concept of cells seems to be useful in 3D displaying [15]. Screen cells are logical structures whose location and shape are determined by light sources, one of which is at the center of a cell. (Here and in the next sentence, the orthogonal layout is referred to.) A cell can be defined as an area of the screen, all the points of which lie closer to its own center than to any other center. From this point of view, the layout of the light source array can be said to be distinctive because it defines the layout of the screen cells. For example, a regular array in which the light sources are located equidistantly by horizontal rows and vertical columns (Fig. 1a) generates an array of square cells (Fig. 1b).

Other layouts of light sources generate different cell structures. Among all the options, two regular ones should be mentioned. A light source array of equidistant horizontal rows, with each next row displaced by a half-period (Fig. 2a), generates hexagonal cells (Fig. 2b) whereas an array of non-equidistant rows with or without half-period displacements (Fig. 2c) generates triangular cells (Fig. 2d).

Among these structures, Fig. 1b, 2b, and 2d show regular tessellations (tilings) denoted as 4^4, 6^3, and 3^6, respectively. It is known that with the exception of these three (square, hexagonal, and triangular tessellations), there is no other way to fill the plane with regular polygons. Note that tessellations 6^3 and 3^6 are mutually dual while 4^4 is self-dual. In addition, by stretching the squares, tessellation 4^4 (Fig. 1b) can be transformed into a rectangular tessellation of rhomboidal cells.

It is essential to note that the light sources lie exactly at the centers of the corresponding cells in one case only, for the orthogonal layout. Otherwise (almost always), they lie at the projected (displaced) centers of the cells, as if they

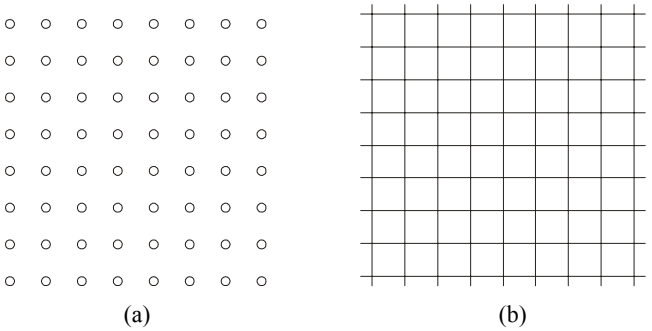

Fig. 1. Light source array and the corresponding screen cells.

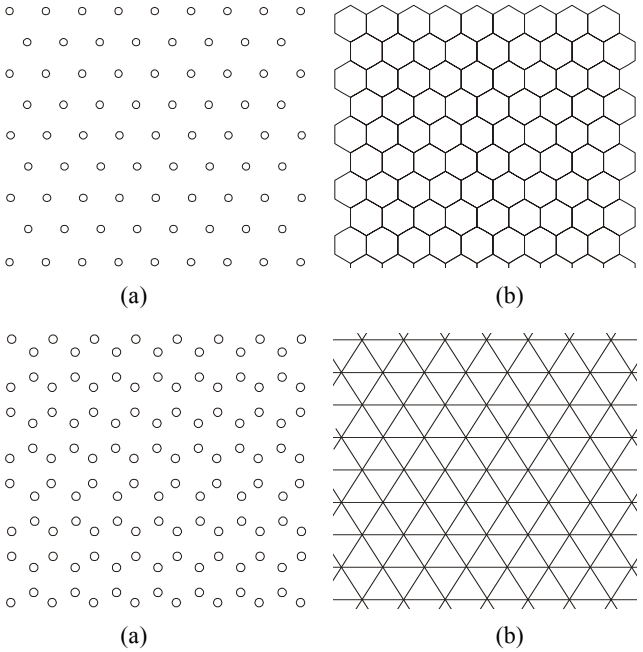

Fig. 2. More light source arrays and the corresponding regular cells.

are observed from the observer region. Effectively, this means that in contrast to the orthogonal case, the scale factors are different for the plane of light sources and for the image plane.

Although it is known that 3D displays can be built based on random structures [17], this feature was not taken into account in the current study. Moreover, there must be a certain distance between two layers in 3D displays. In this study, only parallel layers and cells distributed periodically (regularly) were considered.

Due to the physical limitations of displays, only two of three regular tessellations can be used: the square and hexagonal tessellations. Otherwise, in the attempt to implement triangular tessellation 3^6, a reflection transformation would have had to be applied alternately (to even or odd cells). Alternatively, an attempt may be made to use semiregular tilings and probably even non-uniform (demiregular) ones. These can constitute intermediate cases between regular and random structures in 3D displays.

3. Main Regions

A display device has at least two important areas: that where the images are displayed and that where the images are preferably observed. In the theoretical geometric description of an autostereoscopic 3D display, these are re-

ferred to as the observer and image regions.

The observer region is defined as a space in front of a display from which all the light sources are visible through the corresponding (nearest) cells. The visibility of the light sources can vary at least for two reasons: their limited (or non-uniform) angular luminosity and the lateral displacement of an observer with a non-zero distance between layers. The central part of the region (the diagonal in a cross-section) used to be known as a sweet spot as it provides the best visual image.

The image region is defined as a space for displayed visual images for an observer located at the main diagonal of the observer region (sweet spot). The image region is an analog of viewing frustum in 3D computer graphics. It occupies the screen together with the adjacent rooms in front and behind it. In this study, only the quasihorizontal cross-sections of the regions were considered. The main diagonal of the image region lies in the same plane as a row of an array of light sources and observer eyes. This means that there should exist at least one horizontal row in the array.

In the cross-section, both regions have the shape of a deltoid (kite), a quadrilateral comprised of two adjacent equilateral triangles. Only one of the two regions can be finite or closed (see Fig. 3).

The origin is located at the intersection point of the diagonals of the trapezoid with parallel bases *a* and *b* (Fig. 3). For the distances from the origin to the bases of the trapezoid (Fig. 4), the following formulas were derived:

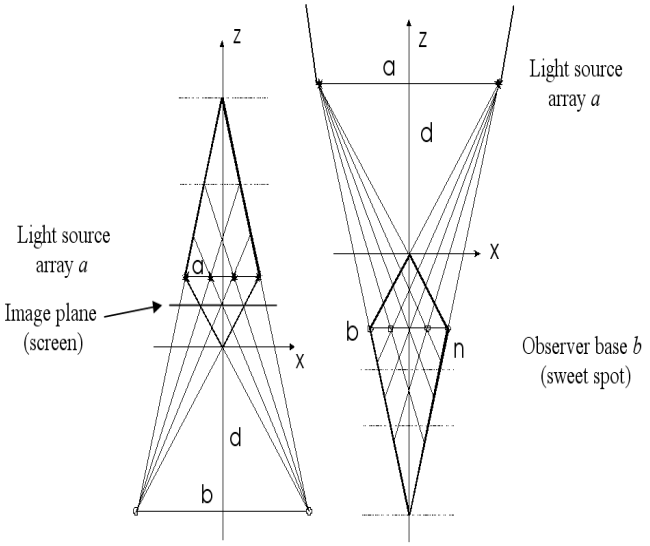

Fig. 3. Layout of the regions depending on *c*: (a) Finite image region, *c*>1. (b) Finite observer region, *c*<1.

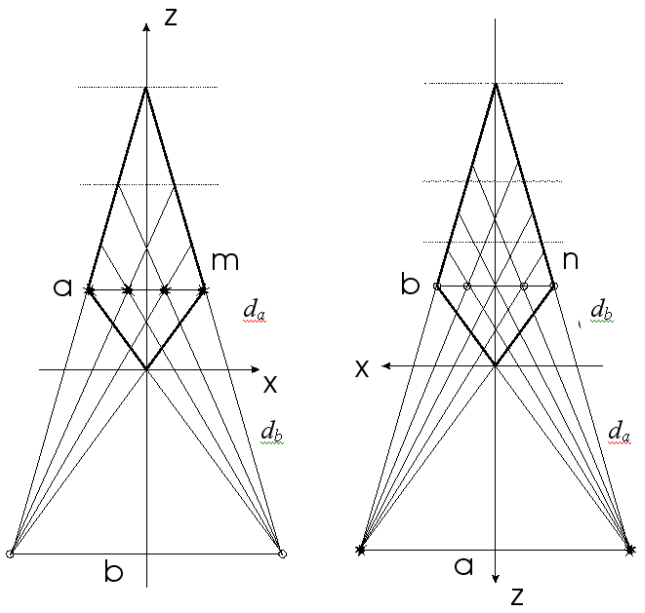

Fig. 4. Regions in the "similar" position (as in Fig. 3, the observer region is rotated 180°).

$$d_a = \frac{1}{c+1} d$$
$$d_b = \frac{c}{c+1} d \quad , \tag{1}$$

where *a* is the width of the light source array and *b* is the width of the observer region (both in the same cross-section), *d* is the distance between them, and $d_a + d_b = d$.

There is an important ratio that characterizes the finiteness of the regions in the geometric description. The three possible cases may be referred to as converging, diverging, and parallel layouts of the regions. The geometric characteristic can be defined as follows:

$$c = \frac{b}{a}. \tag{2}$$

The value of *c* is distinctive (i.e., less, greater, or equal to one), and it defines the converging, diverging, or parallel layout, two of which are shown in Fig. 3.

As a well-defined similarity in the description of the two regions will be found in this section, it is enough to consider one of them. This can be understood from Fig. 4, where the two regions are shown to be in the position "above the origin."

As can be observed from Fig. 4, the substitution of the variables

$$\begin{array}{ll} a \leftrightarrow b & x \leftrightarrow -x \\ m \leftrightarrow n & z \leftrightarrow -z \end{array}, \tag{3}$$

and consequently,

$$c \leftrightarrow c^{-1} \quad , \tag{4}$$

transforms the formulas for one region into another. For example, for the period of the nodes of the image region,

$$w_a(i) = \frac{1}{m(c+1)-i} b \, . \tag{5}$$

The corresponding formula (obtained independently or by applying (3) and (4) above) is valid for the observer region

$$w_b(i) = \frac{1}{n(c^{-1}+1)-i} a \, . \tag{6}$$

4. General Formulas

In this section, only the image region is considered, assuming an easy conversion of all the formulas to the observer region using (3) and (4). The notation is as follows:

$$m = N^* - 1,$$

where N^* is the number of light sources in the array along the width diagonal of the region, and i is the running index of the nodal line $i = 0, \ldots, 2m$. In other words, m is the number of line segments between the light sources into which the main diagonal of the region (array a) is subdivided (Fig. 4a).

When counting the total numbers of nodal lines, subregions, and nodes within the main region, note that the total number of lines includes two lines touching the region at the single point (i.e., at the origin and at the farthest vertex):

$$\begin{aligned} N_a^l &= 2m+1 \\ N_a^s &= m^2 \\ N_a^n &= (m+1)^2 \end{aligned} \quad . \tag{7}$$

The number of subregions along the segment of the i-th nodal line within the region is

$$N_a(i) = m - |m-i| \, . \tag{8}$$

As can be seen below, many formulas for the image region will involve the same expression in the denominator. Therefore, it is useful to refer to it as the characteristic function of the image region, as below.

$$f_a(i,m,c) = m(c+1) - i \, . \tag{9}$$

The characteristic function is a function of the three arguments i, m, and c, but in the most practical cases, the second and third arguments may be treated as parameters, and a shortened notation may be used, as below.

$$f_a(i) = m(c+1) - i \, . \tag{10}$$

Note that the denominators in (5) and (6) are characteristic functions of the corresponding regions. Function (10) is always non-negative for $i \in [0, m]$. For the larger $i \in [m+1, 2m]$, its zero gives the index corresponding to the infinite location of the nodal line for a non-closed region:

$$i_a^{\infty} = m(c+1) \quad . \tag{11}$$

Therefore, the maximum available index in Euclidean coordinates is

$$i_a^{\max} = m + [m \min(1,c)], \tag{12}$$

where the square brackets mean the integer part. The location of the nodal line and the width of the segment of the i-th nodal line falling within the region are

$$l_a(i) = \frac{i}{f_a(i)} d_b = \frac{i}{f_a(i)} \frac{c}{c+1} d \tag{13}$$

$$W_a(i) = w_a(i) \cdot N_a(i) = \frac{m - |m-i|}{f_a(i)} b . \quad (14)$$

The distances between the successive lines and between the previous and next lines (height of the subregion) are

$$\Delta l_a(i) = l_a(i+1) - l_a(i) = \frac{mc}{f_a(i)(f_a(i)-1)} d , \quad (15)$$

$$h_a(i) = l_a(i+1) - l_a(i-1) = \frac{2mc}{f_a^2(i)-1} d . \quad (16)$$

The area of the subregion equals

$$s_a(i) = \frac{1}{2} w_a(i) h_a(i) = \frac{mc}{f_a(i)(f_a^2(i)-1)} bd . \quad (17)$$

The slope of the side is

$$\tan \alpha_a(i) = \frac{\Delta l_a(i)}{w_a(i)/2} = \frac{2m}{f_a(i)-1} \frac{d}{a} . \quad (18)$$

4.1 Neighbors of the main diagonal

In this case,

$$i = m \pm 1, \; N_a(m \pm 1) = m - 1, \text{ and}$$
$$f_a(m \pm 1) = mc \mp 1 . \quad (19)$$

The formulas for $l_a(m \pm 1)$, $\Delta l_a(m \pm 1)$, and $w_a(m \pm 1)$ were obtained from [18]. Using (19), the formulas for width, height, area, and slope can also be found, as follows:

$$W_a(m \pm 1) = \frac{m-1}{mc \mp 1} b = \frac{m-1}{mc \mp 1} ca , \quad (20)$$

$$h_a(m \pm 1) = \frac{2}{mc \mp 2} d , \quad (21)$$

$$s_a(m \pm 1) = \frac{1}{(mc \mp 1)(mc \mp 2)} bd = \frac{c}{(mc \mp 1)(mc \mp 2)} ad , \quad (22)$$

$$\tan(\alpha_a(m \pm 1)) = \frac{2m}{mc \mp 1 - 1} \frac{d}{a} = \begin{cases} = 2c \dfrac{a}{d} = \dfrac{b}{d}, i = m-1 \\ = 2 \dfrac{mc-2}{m} \dfrac{a}{d}, i = m+1 \end{cases} . \quad (23)$$

Formulas (20)-(23) are meaningful at least for two reasons: the preferable location of the screen in the image region is one of the neighbors, and the size of the sweet spot in the observer region is also defined by the neighbors.

4.2 The screen

A very important particular case is the screen (light-emitting or transparent). To implement a display device using the model, the screen location must be known. By definition, the screen is located in the image region. This location is the same for single and multiple regions. Basically, the screen can be located either in front or behind the screen (Fig. 5), although generally speaking, combined dual-screen displays satisfying the same geometric relations are also possible. The centers of screen cells (see section 2) are also shown in Fig. 5 for one of the screen locations.

In the image region, the screen used to be located one nodal line before (or after) the light source array. (In the case of lenslets, there are additional conditions: the focal distance should be equal to the distance between the lens and the screen, and distance *d* should be derived from the lens formula.) These two special locations do not point to a necessary requirement, and principally, any other distance is not prohibited. In such case, however, either there will be some unused area in all the cells or the cells may overlap with one another. Locating the screen at the ±1st nodal line from the array ensures the best utilization of the screen area.

This geometry principally allows even combined dual-screen displays, in which light-emitting and transparent screens are located at the two sides of the pinhole array (as *m*+ and *m*- in Fig. 5), filling their planes with proper gaps to be filled from another image plane so that the cells of both layers together effectively fill the whole plain. This principally allows the use of tessellations with a 180° rotation, such as tessellation 3^6, which cannot be used otherwise (section 2).

For the variables related to the screen, the following special notation was used, among others:

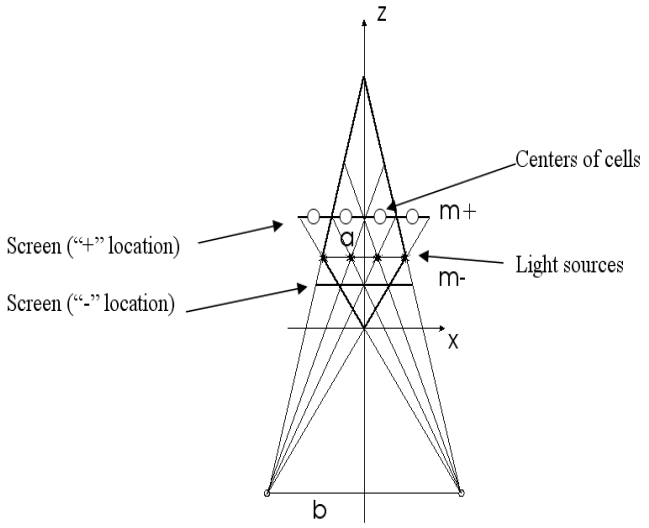

Fig. 5. Two possible locations of the screen and the centers of the cells.

$$\begin{aligned} \Delta l_{m+} &= \Delta l_a(m) \\ \Delta l_{m-} &= \Delta l_a(m-1) \\ W_{m\pm} &= w_a(m\pm 1)\cdot N_{m\pm} \\ h_{m\pm} &= h_a(m\pm 1) \end{aligned} \quad . \tag{24}$$

For both preferable screen locations, $i = m \pm 1$ (lines m+ and m- in Fig. 5), the screen extends the side boundaries of the image region. As such, the general formula for N and the related formulas may be invalid for the screen and thus need corrections. In particular, the number of nodes $N_{m\pm}$ is not equal to $N_a(m\pm 1)$, as in (8). Instead,

$$N_{m\pm} = N_a(m\pm 1) + 2 = m + 1 . \tag{25}$$

The width of the screen and its distance to the main diagonal [18] equal

$$W_{m\pm} = \frac{m+1}{mc\mp 1} b = \frac{m+1}{mc\mp 1} ca , \tag{26}$$

$$\Delta l_{m\pm} = \frac{1}{mc\mp 1} d . \tag{27}$$

The formulas for $f_{m\pm}$, $l_{m\pm}$, $w_{m\pm}$, $h_{m\pm}$, $s_{m\pm}$, and $\alpha_{m\pm}$ literally match the corresponding general ones for $f_a(m\pm 1)$, $l_a(m\pm 1)$, etc. They were thus not included.

5. Multiple Regions

The multiple observer regions were previously considered [18]. With the necessary conditions [19] satisfied, these regions in projective form [16] can be extended periodically across the half-plane (Fig. 6) along the x and z axes, and non-periodically across the whole plane [16].

Corresponding to the multiple observer regions are their image counterparts, which all together constitute a set of multiple image regions. The useful periodicity of the observer regions, however, does not work with the image region. This is because of the common base (main diagonal) of all the image regions whereas the multiple observer regions, on the contrary, have displaced bases (b_{-1}, b, and b_{+1} in Fig. 6). This accounts for the principal difference in their geometry. An example for three image regions is shown in Fig. 7. This illustration involves only one base a, but again, several (three) bases b_i. In this figure, two side regions are

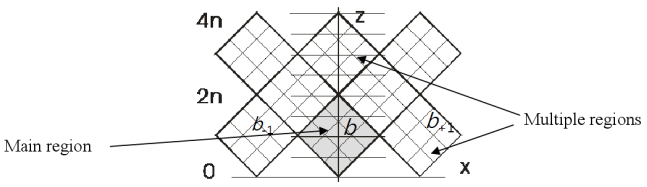

Fig. 6. Periodic extension of observer region b in two directions (projective form).

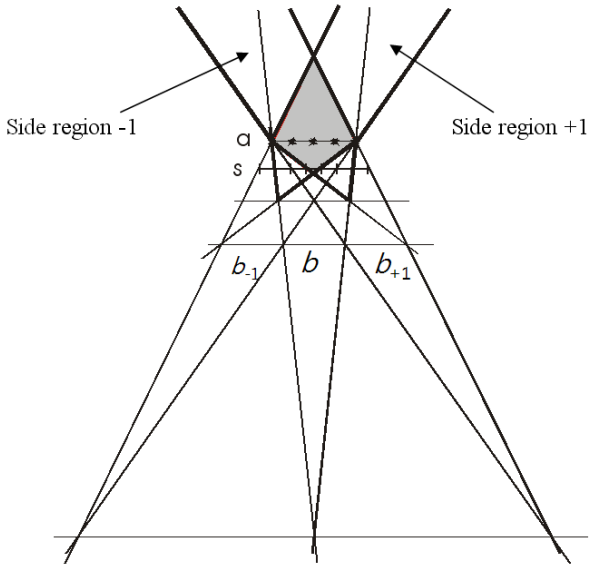

Fig. 7. Three image regions and their common area.

highlighted along with the common area of all the three regions.

The common area of all the image regions is shown in Fig. 7. Although the image regions in this illustration are infinite (the observer regions are finite, as indicated in section 3), their common area is finite. More generally, it can be finite when

$$Mc > 1, \tag{28}$$

which may be valid for the sufficiently large M and even for $c<1$.

The projective form does not change this. Even if a single region can be made a square using a properly chosen arbitrary constant, other image regions will be skew figures (i.e., parallelograms). Nevertheless, there are at least a couple of advantages in their position: the projected common area is a rhomb, and the nodal lines are equidistant (see Fig. 8).

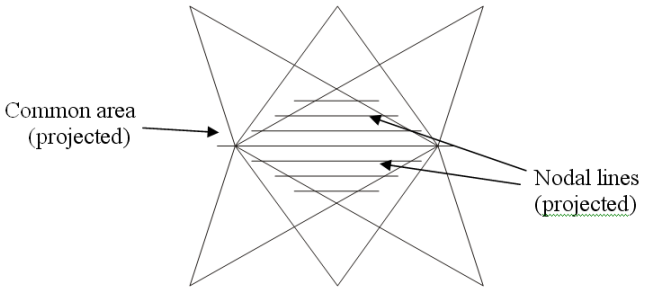

Fig. 8. Multiple image regions from Fig. 7 in projective form.

6. Conclusion

In this study, a relationship between the light source array and the screen cells was found. The image and observer regions were considered, including the multiple ones. The case of the single regions was analyzed in detail, while the multiple regions and projective representation were analyzed more briefly. For the screen location, as it is one of the most important locations in the model, special formulas were obtained for it.

The image and observer regions in 3D displays were considered. At the same time, the theoretical model was used for quality estimate [20] and distance measurements [21], demonstrating a good agreement between the theoretical and experimental data. In particular, the integral geometric estimate for the visual quality of 3D displays [20] was basically inspired by the equivalents of equations (13)-(16) for the observer region, by the geometric layout, and by the experimental results of other authors referred to in [20]. It describes the common characteristics of individual views (i.e., how they behave together). The projective representation of the quality estimate is expressed in the convenient piecewise linear graph of the quality function. [21] describes the method of measurement of the geometric parameters of autostereoscopic 3D displays. Similar to the quality estimate, it is also based on the projective transformations. In the experiments, the optimal distance was measured using the improved testing patterns, which provide higher accuracy for integer image cells. The measurement results do not depend on the trajectory along which a measuring instrument approaches the screen.

Compared to the previous studies, in this study, three layouts of light source arrays were additionally analyzed, along with their regular tessellations. The characteristic function (10), which is used in many formulas across the model, was introduced. Formulas for the areas and angles were added. Two particular cases (neighbors and the screen) were considered in detail. A dual-screen configuration based on the triangular tessellation was proposed. Moreover, the method of transforming the formulas from one region to another was formulated. The geometric dissimilarity between the multiple observer and image regions was also found.

In this paper, only the quasihorizontal cross-sections of the regions are considered, and not their spatial structure. Nevertheless, it is hoped that a spatial structure can be built based on these authors' previous [16, 19], current, and further developments of the model. Some new general properties of 3D displays may affect the display development, especially the invention of new 3D display methods. In the further research, these authors intend to take into account more new features, such as sight direction, which is important in tracking the observer eyes, as in [22], or in finding visual-attention regions, as in [23]. Also, various non-ideal conditions will be included in the model.

References

[1] M. Halle, *Computer Graphics*, **31**, 58 (1997).
[2] N.A. Dogdson, *Computer*, **38**, 31 (2005).
[3] G.J. Woodgate and J. Harrold, in *Proc. EuroDisplay* (2005), p.24.

[4] A. Kubota, A. Smolic, M. Magnor, M. Tanimoto, T. Chen and C. Zhang, *IEEE Signal Processing*, **24**, 10 (2007).

[5] L. Onural, T. Sikora, J. Ostermann, A. Smolic, M.R. Civanlar and J. Watson, in Proc. National *Association of Broadcasters Broadcast Engineering Conference*(*NAB BEC*) (2006), p.456.

[6] P. Martinez-Cuenca, G. Saavedra, M. Martinez-Corral and B. Javidi, in *Proc. IEEE* **97**, (2009) p. 1067.

[7] J.-H. Park, K. Hong and B. Lee, *Appl. Opt*., **48**, H77 (2009).

[8] Y. Kim, K. Hong and B. Lee, *3D Research*, **1**, 010102-1 (2009).

[9] S. Manolache, A. Aggoun, M. McCormick and N. Davies, *J. Opt. Soc. Am. A*, **18**, 1814 (2001).

[10] J. Bi, D. Zeng, Z. Zhang and Z. Dong, in Proc. *World Congress on Computer Science and Information Engineering* (2009), p. 514.

[11] A. Stern and B. Javidi, in *Proc. IEEE*, **94**, (2006), p. 514.

[12] G. Baasantseren, J.-H. Park and N. Kim, in *Proc. Proceedings of the Conference on Lasers and Electro-Optics* (*CLEO/Pacific Rim*) (2009), p. ThJ1-2.

[13] J. Kim, Y. Kim, H. Choi, S.-W. Cho and B. Lee, in *Proc. Proceedings of the Conference on Lasers and Electro-Optics* (*CLEO/Pacific Rim*) (2007), p. ThP_104.

[14] D.-H. Shin, B. Lee and E.-S. Kim, *ETRI Journal*, **28**, 521 (2006).

[15] V. Saveljev and S.-J. Shin, *J. Opt. Soc. Korea*, **13**, 131 (2009).

[16] V. Saveljev, accepted for 10th *International Meeting on Information Display* (*IMID*), Seoul, Korea (2010).

[17] M.D. Panah, B. Javidi and E.A. Watson, *Opt. Express*, **16**, 6368 (2008).

[18] V. Saveljev, in *Proc. Joint Workshop on the Optical Information Processing and Three-Dimensional Display Technology*, Gangwon, Korea, (2009), p. 101.

[19] V. Saveljev, in Proc. *17th Conference on Optoelectronics and Optical Communications*(*COOC*), Gangwon, Korea (2010), p. 224.

[20] V. Saveljev, in *Proc. 20th Workshop on Optical Technology: 3D Imaging, LED and Solar Technology*, Chungbuk, Korea (2010), p. 73.

[21] V. Saveljev, in *Proc. Winter Annual Meeting of Optical Society of Korea 20th Anniversary*, Daejeon, Korea (2010), p. F3F-VIII3.

[22] Y.-M. Kwon, K.-W. Jeon and S.-K. Kim, in *Proc. SPIE*, **6392** (2006), p. 63920J-1.

[23] M.-C. Park and K. Cheoi, in *LNCS*, **5068** (2008), p. 203.